Journal of

Applied and Computational Mechanics

Shahid Chamran
University of Ahvaz

Research Paper

Optimization of Ventilation Register Locations for Reducing Suspended Particle Concentration Using the Taguchi Method

H. Sajjadi[1,2] ⓘ, S.N. Nabavi[1,2] ⓘ, G. Ahmadi[3] ⓘ, A. Amiri Delouei[1,2] ⓘ, H. Naeimi[1,2] ⓘ

[1] Department of Mechanical Engineering, University of Bojnord, Bojnord, Iran

[2] Center for International Scientific Studies and Collaboration, Ministry of Science, Research and Technology, Tehran, Iran

[3] Department of Mechanical and Aerospace Engineering, Clarkson University, Potsdam, USA

Abstract. In the present study, the Multi-Relaxation Time Lattice Boltzmann method (MRT-LBM) was employed to solve the airflow inside a scaled room model with dimensions of 0.914×0.457×0.305 m. This room model is considered a representative space with a 1:10 scale to an actual room. The selected room is equipped with a ventilation system. For optimizing the inlet and outlet locations of the airflow, 32 different positions in terms of length, width, and height for the inlet and 4 positions for the outlet were considered. The Taguchi method was utilized for optimizing the inlet and outlet locations, reducing the required number of experiments from 128 to 16. To assess the number of suspended particles, 86400 particles with a size of 1μm were injected into the room. Then, the particle behaviors were examined for a total duration of 60 seconds. The obtained results indicate that the location of the air conditioning system significantly influences the concentration of airborne particles responsible for disease transmission. Utilizing the Taguchi optimization method, optimal positions for the inlet and outlet air were determined to minimize the number of suspended particles in the room (the best position) and maximize it (the worst position).

Keywords: Optimization, Airborne particles, MRT-LBM, Taguchi method.

1. Introduction

In recent decades, the lattice Boltzmann method (LBM) has gained significant attention for simulating fluid flow and heat transfer [1-3]. This method utilizes the distribution function of fluid particles to simulate the macroscopic properties of the flow. In the lattice Boltzmann method, all calculations are explicit, and there is no need to solve any implicit system of equations. Due to the inherently local nature of the calculations, this method can easily be parallelized [4]. Moreover, due to the ease of implementing boundary conditions, the LBM found extensive application in solving fluid flow problems in complex geometries [5, 6]. Many important applications, including fluid flow and heat transfer in turbulent flows, flows with complex boundaries (porous media and moving curved surfaces), multiphase flow, and non-Newtonian fluid flows, were reported in the literature [7-9].

Despite significant advancements over the past century, turbulent flow remains a major challenge for scientists and engineers [10]. Notwithstanding numerous efforts, turbulent flow continues to be an unsolved in physics. Nevertheless, various models were developed to handle practical turbulent flow applications, each valid for specific flow regimes. The Reynolds-Averaged Navier-Stokes (RANS) model has gained much attention in engineering applications due to its low computational cost [11, 12]. However, the RANS method only provides the results of the averaged flow properties and requires modeling of the Reynolds stresses. On the other hand, the Direct Numerical Simulation (DNS) resolves all scales of flows without the need for additional modeling [13]. The DNS, however, requires extensive computational resources, making it difficult and expensive for practical applications. Another method between the RANS and DNS is the Large Eddy Simulation (LES) [14]. This method directly solves large turbulence eddies, while the smaller subgrid scale eddies are filtered and modeled.

Given that most people spend their time in indoor environments, indoor air quality significantly impacts human health. Additionally, the transmission of viral diseases indoors, especially the coronavirus pandemic, which has affected the entire world, maintaining indoor air quality is even more critical [15-21]. Balachandar et al. [15] studied the host-to-host airborne transmission as a multiphase flow. Gorbunov [16] investigated the transfer of aerosol particles produced by coughing and sneezing using computational fluid dynamics (CFD). Bahramian et al. [17] investigated the effect of indoor temperatures and airflow dynamics on the airborne transmission of sneeze droplets in enclosed environments. Bahramian and Ahmadi [18] explored the effect of sneeze flow velocity on respiratory droplet dispersion in confined spaces. Karami et al. [19] studied the spread of COVID-19 infection in a dental clinic. All these studies used 3D computational models, including heat and mass transfer and dispersion of dilute respiratory droplets, to assess aerosols' dispersion in different environments. These simulations demonstrated that the ventilation system and

indoor geometries influenced the dispersion of respiratory aerosols. Furthermore, the results indicated that aerosol particles ranging from 1μm to 100 μm could potentially carry coronavirus viruses and can travel large distances, even up to 30 meters, under certain ventilation conditions. Harish et al. [20] and Mirzaie et al. [21] computationally examined the spread of the coronavirus (COVID-19) virus in ventilated classrooms. Their results showed that the speed of sneeze and cough droplets initially decreases as they move away from the emitter mouth and then increases as they approach the exhaust. It is also observed that sneeze droplets spread to a greater distance compared to cough droplets due to higher initial speeds. The studies of cough and sneeze droplets spreading indicate that a social distance of 2 meters is the minimum that should be maintained to prevent virus spread, and it may not be sufficient for certain conditions.

Mofakham and Ahmadi [22] studied the accuracy of discrete and continuous random walk models to simulate particle dispersion and deposition in turbulent flows and the effects of velocity fluctuations on particle motion. They suggested improved continuous random walk (CRW) and discrete random walk (DRW) models for accurately predicting the particle concentration and deposition. Ahmed et al. [23] discussed the importance of studying how droplets are transported when people speak and exhale in connection to the COVID-19 pandemic. They reported that the airflow jet at the mouth during speaking is unstable, and its angle fluctuates significantly. They also reported that the airflow speed at the lips when making certain sounds is faster than previously thought and is not steady. These results indicated that previous studies on air movement during speech have not fully accounted for how far respiratory droplets can travel. This is important for understanding how respiratory diseases like COVID-19 spread. Mofakham et al. [24] used direct numerical simulations of expiratory flow during sustained fricative utterances. Their results improved the understanding of how respiratory droplets are expelled during speech. Mofakham et al. [25] worked on respiratory particle propagation during fricative productions and the effect of airflow variations on particle transport and dispersion as a function of particle size. Their results illustrated significant effects of the airflow jet trajectory variations on the pattern of particle motion and transport during fricative utterances. Obeid et al. [26] used a 3-D computational model to solve the airflow inside a ventilated room. They concluded that enhancement in the hourly air change rate from 2.0 to 5.6 declined the 1 μm droplet concentration inside the room by a factor of 2.8 and in the breathing zone of the receptor occupant by a factor of 3.2. Karami et al. [27] simulated the cough droplet motion using the Eulerian-Lagrangian CFD model. They showed that the air ventilation layout strongly affects the droplet motion in the indoor space, and the air-curtain flow pattern significantly reduces the transportation of virus-infected cough droplets. Motosami et al. [28] investigated the impact of cough dynamics on safe social distancing in an indoor environment using The CFD approach. The findings suggest that, in general, women have a smaller contamination area because of their lower cough velocities and droplet emissions. Furthermore, a significant portion of respiratory droplets from unobstructed coughing spread more than the two-meter social distancing threshold. Ahmadzadeh and Shams [29] numerically studied the spread of infectious diseases in a meeting room. The main objective of their study was to examine the effects of window opening frequency, outlet layout, and the location of air conditioning systems on particle dispersion. In their study, two wall-mounted air conditioning units are installed on the back or front wall side. Their results indicated that reducing the distance between the installed ventilation systems and the ceiling can reduce suspended particles by more than 35%. Xu et al. [30] investigated the movement and settling patterns of small particles in turbulent Rayleigh–Bénard convection using 2D simulations at a Rayleigh number (Ra) of 108 and a Prandtl number (Pr) of 0.71, corresponding to air. They employed a Lagrangian point particle model to track particle behavior in turbulent flow conditions. Their findings revealed that under different Stokes numbers (St), particles exhibited varied distributions: homogeneous for St < 10^{-3}, band clustering for $10^{-3} \leq$ St $\leq 10^{-2}$, and rapid sedimentation at higher St values. Analysis of mean-square displacement showed distinct motion regimes over time intervals, reflecting both isotropic and anisotropic characteristics. Moreover, a phase diagram illustrating particle deposition locations on the wall demonstrated three distinct states based on particle properties, with a notable tendency for particles to deposit near vertical walls adjacent to hot plumes.

In many problems, the design of experiments (DOE) is done to reduce the cost and the testing time to reach the optimal number of experiments. DOEs are divided into full factorial designs and Fractional Factorial Designs [31, 32]. In the full factorial design, all possible combinations of the parameters are examined. However, Taguchi's method [33, 34], one of the fractional factorial methods, provides an optimal minimum number of needed experiments. Taguchi's method combines statistical and mathematical methods used in experimental design. This method determines the optimal conditions for the input parameters with a minimum number of experiments. The reduction in the time and cost of experiments are the main advantages of the Taguchi method.

The presented literature survey shows that studies of optimizing the ventilation register locations to minimize the spread of particles in a room are scarce. Hence, this study examined the impact of the inlet and outlet air register locations on particle dispersion and transport. The Taguchi method was used, and the optimal locations of the ventilation inlet and outlet registers for mitigating particle dispersion in the room were evaluated.
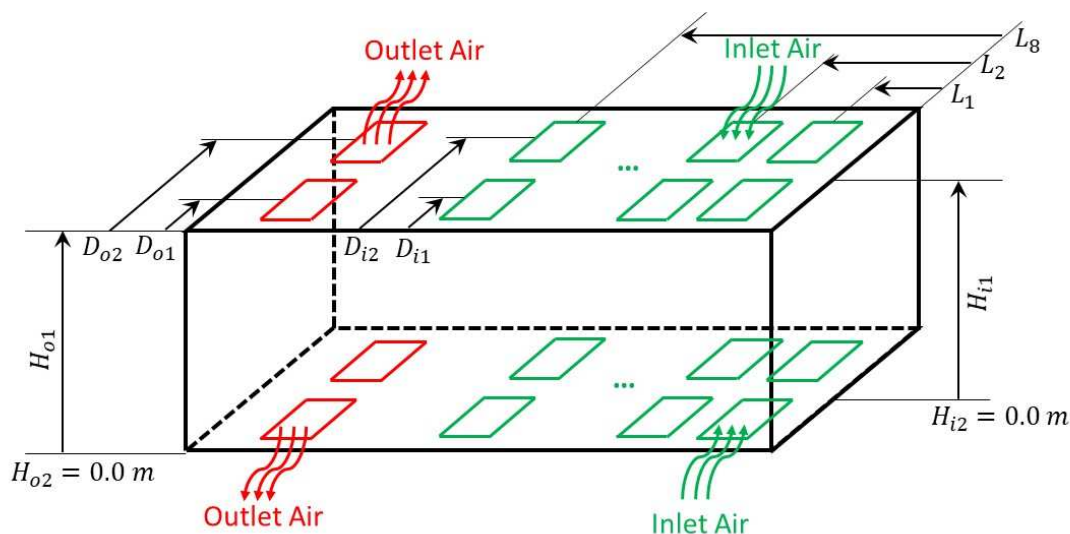

Fig. 1. Scaled room geometry and the studied locations of inlet and outlet.

Table 1. The coordinates of the geometric parameters of the inlet and outlet.

D_1	0.164 (m)
D_2	0.392 (m)
L_1	0.056 (m)
L_2	0.123 (m)
L_3	0.190 (m)
L_4	0.257 (m)
L_5	0.324 (m)
L_6	0.391 (m)
L_7	0.458 (m)
L_8	0.525 (m)

Table 2. Boundary conditions.

Boundary	Type of Boundary condition
Inlet	Velocity inlet
Outlet	Pressure outlet
Wall	No slip

2. Room Geometry

This study investigated a modeled room with a scaling ratio of 1:10, with one inlet and one outlet, as shown in Fig. 1. The room model dimensions are 0.914×0.457×0.305 meters. The room inlet and outlet dimensions are the same and equal to 0.101×0.101 meters.

As expected, the location of inlets and outlets of the airflow can significantly impact the room's ventilation and, consequently, the particle dispersion and transport in the room [9]. Various airflow inlet and outlet locations in the room's ceiling and floor are examined here. Figure 1 shows a schematic of the room and the locations of the airflow inlets and outlets studied. There are two rows of eight locations for the inlet on the ceiling and floor. Here, L_i is the distance of the inlet center from the room's right wall. D_i is the distance of the inlet center from the room wall, as shown in Fig. 1. There are only four positions for the outlet (two on the ceiling and two on the floor) near the room's left wall. The values of the parameters shown in Fig. 1 are listed in Table 1. Therefore, there are 32 positions for the air inlet and only four for the airflow outlet. The airflow Reynolds number is 1500 based on the length of the inlet and the inlet airflow velocity. The air density is 1.18 kg/m³, and the air kinematic viscosity is 5.10×10⁻⁵ m²/s. The airflow is incompressible and Newtonian. In addition, the airflow is turbulent, and the LES model is used to simulate the airflow field. The boundary conditions used in the present work are listed in Table 2. For the particles, the trap boundary condition is used. So, particles are assumed to be deposited when they reach the walls.

To investigate the particle motion in the room, when the airflow reaches the steady state, 144 particles with a size of 1µm with a time interval of 0.05 seconds are injected from the inlet (with the same velocity as the inlet air) into the room for 30 seconds (86400 particles), and the particle behavior is examined for 60 seconds.

3. Numerical Solution

3.1. Multi Relaxation Time Lattice Boltzmann method using the LES model (MRT-LBM-LES)

Considering the increased stability of the MRT method, this approach was utilized in the current study. Based on this method, for the D3q19 lattice (Fig. 2), the following equation can be used to calculate the distribution function for the velocity [35]:

$$f_i(x + c_i\Delta t, t + \Delta t) = f_i(x,t) - M_{ij}^{-1}.\hat{S}_{jk}.[R_k(x,t) - R_k^{eq}(x,t)] \tag{1}$$

Equation (1) represents the particle velocity, which is expressed as follows for the D3Q19 lattice:

$$c_i = \begin{cases} (0,0) & i = 0 \\ c(\pm 1,0,0), c(0,\pm 1,0), c(0,0,\pm 1) & i = 1-6 \\ c(\pm 1,\pm 1,0), c(\pm 1,0,\pm 1), c(0,\pm 1,\pm 1) & i = 7-18 \end{cases} \quad \text{for} \quad D3Q19 \tag{2}$$
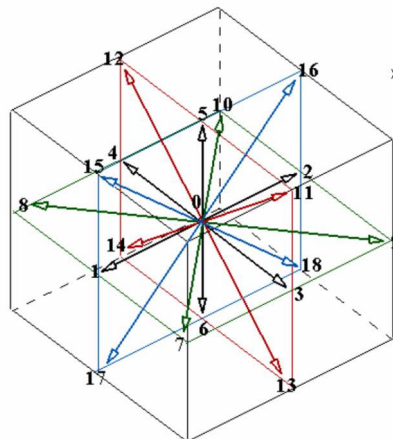
Fig. 2. D3Q19 lattice.

in which $c = \delta x / \delta t$, where δx and δt are constant length and time interval values, which are considered equal to one. R in Eq. (1) is calculated as: $R = MF$, where F is the matrix of distribution functions (f), and the matrix M is calculated as:

$$M = \begin{pmatrix} 1 & 1 & 1 & 1 & 1 & 1 & 1 & 1 & 1 & 1 & 1 & 1 & 1 & 1 & 1 & 1 & 1 & 1 & 1 \\ -30 & -11 & -11 & -11 & -11 & -11 & -11 & 8 & 8 & 8 & 8 & 8 & 8 & 8 & 8 & 8 & 8 & 8 & 8 \\ 12 & -4 & -4 & -4 & -4 & -4 & -4 & 1 & 1 & 1 & 1 & 1 & 1 & 1 & 1 & 1 & 1 & 1 & 1 \\ 0 & 1 & -1 & 0 & 0 & 0 & 0 & 1 & -1 & 1 & -1 & 1 & -1 & 1 & -1 & 0 & 0 & 0 & 0 \\ 0 & -4 & 4 & 0 & 0 & 0 & 0 & 1 & -1 & 1 & -1 & 1 & -1 & 1 & -1 & 0 & 0 & 0 & 0 \\ 0 & 0 & 0 & 1 & -1 & 0 & 0 & 1 & 1 & -1 & -1 & 0 & 0 & 0 & 0 & 1 & -1 & 1 & -1 \\ 0 & 0 & 0 & -4 & 4 & 0 & 0 & 1 & 1 & -1 & -1 & 0 & 0 & 0 & 0 & 1 & -1 & 1 & -1 \\ 0 & 0 & 0 & 0 & 0 & 1 & -1 & 0 & 0 & 0 & 0 & 1 & 1 & -1 & -1 & 1 & 1 & -1 & -1 \\ 0 & 0 & 0 & 0 & 0 & -4 & 4 & 0 & 0 & 0 & 0 & 1 & 1 & -1 & -1 & 1 & 1 & -1 & -1 \\ 0 & 2 & 2 & -1 & -1 & -1 & -1 & 1 & 1 & 1 & 1 & 1 & 1 & 1 & 1 & -2 & -2 & -2 & -2 \\ 0 & -4 & -4 & 2 & 2 & 2 & 2 & 1 & 1 & 1 & 1 & 1 & 1 & 1 & 1 & -2 & -2 & -2 & -2 \\ 0 & 0 & 0 & 1 & 1 & -1 & -1 & 1 & 1 & 1 & 1 & -1 & -1 & -1 & -1 & 0 & 0 & 0 & 0 \\ 0 & 0 & 0 & -2 & -2 & 2 & 2 & 1 & 1 & 1 & 1 & -1 & -1 & -1 & -1 & 0 & 0 & 0 & 0 \\ 0 & 0 & 0 & 0 & 0 & 0 & 0 & 1 & -1 & -1 & 1 & 0 & 0 & 0 & 0 & 0 & 0 & 0 & 0 \\ 0 & 0 & 0 & 0 & 0 & 0 & 0 & 0 & 0 & 0 & 0 & 0 & 0 & 0 & 0 & 1 & -1 & -1 & 1 \\ 0 & 0 & 0 & 0 & 0 & 0 & 0 & 0 & 0 & 0 & 0 & 1 & -1 & -1 & 1 & 0 & 0 & 0 & 0 \\ 0 & 0 & 0 & 0 & 0 & 0 & 0 & 1 & -1 & 1 & -1 & -1 & 1 & -1 & 1 & 0 & 0 & 0 & 0 \\ 0 & 0 & 0 & 0 & 0 & 0 & 0 & -1 & -1 & 1 & 1 & 0 & 0 & 0 & 0 & 1 & -1 & 1 & -1 \\ 0 & 0 & 0 & 0 & 0 & 0 & 0 & 0 & 0 & 0 & 0 & 1 & 1 & -1 & -1 & -1 & -1 & 1 & 1 \end{pmatrix} \tag{3}$$

The values related to the relaxation time for the geometry under investigation are as follows:

$$\hat{S}_{ij} = \text{diag}(s_0, s_1, ..., s_{18}) \tag{4}$$

$$s_1 = 1.19 \tag{5}$$

$$s_0 = s_3 = s_5 = s_7 = 0. \tag{6}$$

$$s_9 = s_{11} = s_{13} = s_{14} = s_{15} = \frac{1}{(3\nu_t + 0.5)} \tag{7}$$

$$s_2 = s_{10} = s_{12} = 1.4 \tag{8}$$

$$s_4 = s_6 = s_8 = 1.2 \tag{9}$$

$$s_{16} = s_{17} = s_{18} = 1.98 \tag{10}$$

The LES model with the standard Smagorinsky model was used for evaluating ν_t. That is,

$$\nu_t = (C_s \Delta)^2 |S| \tag{11}$$

In this study, the value of C_s was considered to be 0.16 and $\Delta = (\Delta x \Delta y \Delta z)^{1/3}$. To obtain the value of $|S|$, we have:

$$\left| S_{\alpha\beta} \right| = \sqrt{2 S_{\alpha\beta} S_{\alpha\beta}} = \sqrt{2[S_{xx}^2 + S_{yy}^2 + S_{zz}^2 + 2(S_{xy}^2 + S_{yz}^2 + S_{xz}^2)]} \tag{12}$$

$$S_{xx} = -\frac{1}{38\rho}[s_1 h_1^{neq} + 19 s_9 h_9^{neq}] \tag{13}$$

$$S_{yy} = -\frac{1}{76\rho}[2 s_1 h_1^{neq} - 19(s_9 h_9^{neq} - 3 s_{11} h_{11}^{neq})] \tag{14}$$

$$S_{zz} = -\frac{1}{76\rho}[2 s_1 h_1^{neq} - 19(s_9 h_9^{neq} + 3 s_{11} h_{11}^{neq})] \tag{15}$$

$$S_{xy} = -\frac{3}{2\rho} s_{13} h_{13}^{neq} \tag{16}$$

$$S_{yz} = -\frac{3}{2\rho} s_{14} h_{14}^{neq} \tag{17}$$

$$S_{xz} = -\frac{3}{2\rho} s_{15} h_{15}^{neq} \tag{18}$$

$$h_\alpha^{neq} = R_\alpha - R_\alpha^{eq} \tag{19}$$

3.2. Particle motion

The general equation of particle motion is as follows:

$$\frac{du_i^p}{dt} = \frac{1}{\tau_p} \frac{C_D \, \mathrm{Re}_p}{24} \left(u_i^f - u_i^p\right) + \left(1 - \frac{1}{S}\right) g_i + n_i(t) \tag{20}$$

In Eq. (20), u_i^p is the particle velocity in the i-direction and is given as: $u_i^p = dx_i / dt$, u_i^f is the instantaneous fluid velocity in the i-direction as evaluated from the MRT-LBM-LES, $\mathrm{Re}_p = d u_{rel} / \nu$ is the Reynolds number, where $u_{rel} = |u_j^f - u_j^p|$ is the relative velocity magnitude, S is the particle to fluid density ratio, g_i is the acceleration of gravity, and $n_i(t)$ is the Brownian force per unit particle mass. The first term on the right-hand side of Eq. (20) represents the drag force per unit mass of the particle, in which the particle relaxation time is given as:

$$\tau_p = \frac{S d^2 C_c}{18\nu} \tag{21}$$

Here, S is the ratio of particle density to fluid density, and C_c is the Cunningham correction factor, which is given by:

$$C_c = 1 + \frac{2\lambda}{d}(1.257 + 0.4 e^{\frac{-1.1d}{\lambda}}) \tag{22}$$

Here, d is the particle diameter, and λ is the air mean free path is equal to 7×10^{-8}. C_D is the drag coefficient and is obtained from the following relationship:

$$C_D = \frac{24}{\mathrm{Re}_p} \qquad \mathrm{Re}_p < 1$$
$$C_D = \frac{24}{\mathrm{Re}_p}(1 + 0.15 \mathrm{Re}_p^{0.687}) \qquad 1 < \mathrm{Re}_p < 400 \tag{23}$$

The second term on the right-hand side of Eq. (20) represents the effect of gravitational force and buoyancy force, and the last term is the random Brownian force, which can be calculated from the following equation [36] at every time step:

$$n_i(t) = \zeta_i \sqrt{\frac{\pi S_1}{\Delta t}} \tag{24}$$

Here the spectral intensity of the Brownian excitation is given by:

$$S_1 = \frac{216 \nu k_b T}{\pi^2 \rho d^5 S^2 C_c} \tag{25}$$

Here, ζ_i is a zero mean, unit variance, independent Gaussian random number, T is the temperature, ν is the kinematic viscosity, and ρ is the fluid density and k_b is the Boltzmann constant and equal to 1.38×10^{-23}. In the present simulations, the effect of sub-grid scale fluctuations are neglected.

3.3. Design of Experiment (DOE)

To study the effects of the five introduced parameters, which are shown in Table 1 and Section 2, one of which has eight levels and the others have two levels, there are 8×2×2×2×2 = 128 possible combinations of experimental positions. Conducting this number of numerical experiments is very time-consuming and computationally expensive. Using the standard orthogonal array L_{16}, which is suitable for designing experiments with five parameters and different levels, the number of experiments can be significantly reduced to 16. Table 3 shows the L_{16} orthogonal array for designing experiments to optimize the air ventilation system for the room. The numbers in the table indicate the level of each parameter.

Table 3. L_{16} Taguchi orthogonal array.

Design number (DN)	L_i	D_i	H_i	D_o	H_o	Design number (DN)	L_i	D_i	H_i	D_o	H_o
1	1	1	1	1	1	9	5	1	2	1	2
2	1	2	2	2	2	10	5	2	1	2	1
3	2	1	1	1	1	11	6	1	2	1	2
4	2	2	2	2	2	12	6	2	1	2	1
5	3	1	1	2	2	13	7	1	2	2	1
6	3	2	2	1	1	14	7	2	1	1	2
7	4	1	1	2	2	15	8	1	2	2	1
8	4	2	2	1	1	16	8	2	1	1	2

Table 4. Grid independence study.

	N1	N2	N3	N4
Grid size	210×105×70 (x,y,z)	300×150×100 (x,y,z)	360×180×120 (x,y,z)	390×195×130 (x,y,z)

In this study, all the experiments shown in Table 3 must be simulated, and the particle deposition in the room space must be measured. After conducting the experiments, the results are compared to determine the appropriate level of each parameter to achieve the problem's objective. One of the available tools for analyzing the results of the experiments is the signal-to-noise (S/N) ratio.

3.4. Signal-to-noise (S/N) ratio analysis

In the Taguchi method, the parameters or variables of the problem are divided into two groups: controllable and uncontrollable. The controllable factors are those parameters that can be easily controlled and are used to select the best conditions for the problem. The uncontrollable factors are all parameters that may cause changes in the output but are not considered input parameters due to the difficulty of controlling them or insufficient knowledge about them. The S/N ratio indicates the sensitivity of the characteristic under investigation to the input parameters in a controlled process. S/N ratio is related to deviations between experimental data and the desired value using a loss function. The value of this function is chosen among the three states: "the smaller is better," "the closer to the nominal is better," and "the larger is better," depending on the nature of the response function. Taguchi has provided various relationships for calculating the S/N ratio based on the three groups. However, it should be noted that having the highest S/N ratio is always desirable for finding the optimal conditions. High values of the S/N ratio indicate that the effect of controllable parameters is greater than the effect of uncontrollable and noise parameters. The relationships related to the S/N ratio are calculated for each of the states as follows:

$$SN_{LB} = -10\log\left(\frac{1}{n}\sum_{i=1}^{n}\frac{1}{y_i^2}\right) \qquad \text{The larger is better} \qquad (26)$$

$$SN_{SB} = -10\log\left(\frac{1}{n}\sum_{i=1}^{n}y_i^2\right) \qquad \text{The smaller is better} \qquad (27)$$

$$SN_{NB} = -10\log\left(\frac{1}{n}\sum_{i=1}^{n}(y_i - y_o)^2\right) \qquad \text{The closer to the nominal is better} \qquad (28)$$

where n is the number of experiment repetitions, y_o is the desirable value, and y_i is the measured output from the experiment numbers listed in Table 3.

4. Results and Discussion

4.1. Grid independence

A thorough testing was carried out to ensure the solution was not dependent on grid size. Various uniform grids, as listed in Table 4, were used in the present study. The simulation results indicated no significant change in the velocity profile and particle deposition as the grid resolution increased from N3 to N4. Therefore, the N3 grid with 360×180×120 cells were selected for the subsequent simulations.
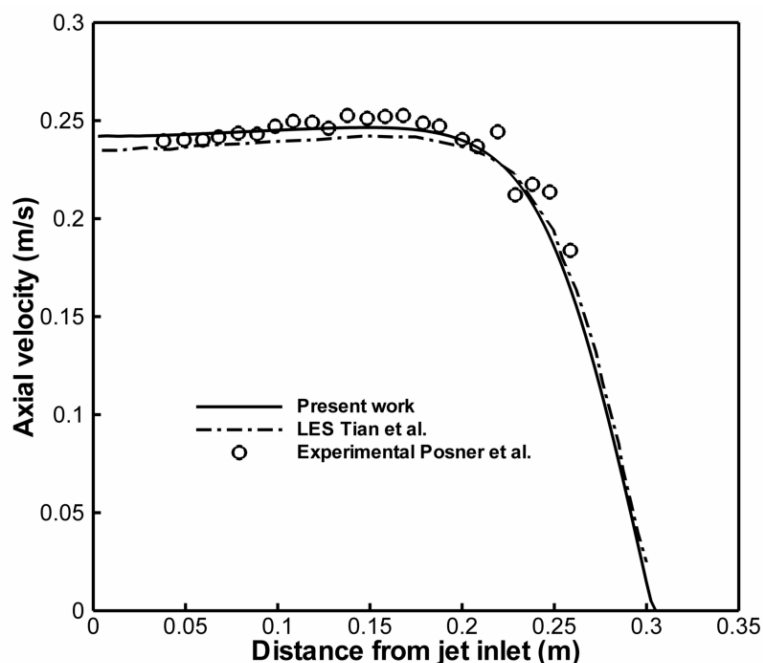

Fig. 3. Comparison of the time-averaged vertical velocity along the inlet axis with the previous results of [37, 38].
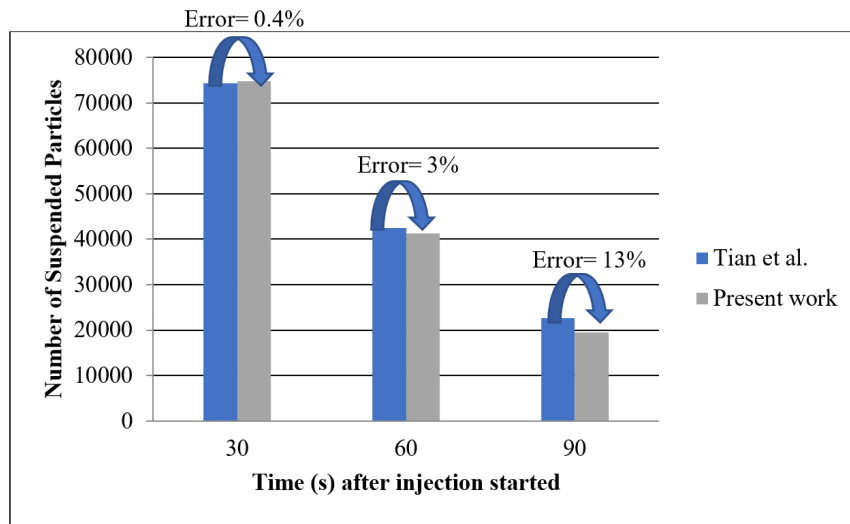
Fig. 4. Comparison of the number of suspended 1 µm particles in the room at different times with the earlier LES simulation of Tian et al. [38].

4.2. Code validation and particle deposition

Since numerical simulation results are required for the optimization analysis and the statistical regression, it is crucial to ensure that numerical simulations capture the physics well. Therefore, the present computational model is verified by comparing its predictions with the experimental data of Posner et al. [37] and LES simulations of Tian et al. [38], who studied a similar room model with the same dimensions for the room and the inlet and outlet registers. In their studies, the inlet and outlet registers were on the ceiling, and a partition was in the middle of the room. In these previous works, when the flow stabilized, reaching a quasi-steady state, 86400 particles were injected into the room from the inlet register with the same velocity as the inlet air for 30 seconds, and then the particle injection was stopped. We simulated airflow and particle dispersion in the room with the inlet airflow and particle injection conditions. The predicted airflow velocity and the number of particles remaining in the room at different times are compared with the results of [37, 38] in Figs. 3 and 4. It is seen that the present simulation results for the velocity profile and the number of suspended particles are in good agreement with the earlier findings.

4.3. Simulation results

In this section, the simulation results obtained for different air inlet and outlet positions, as shown in Table 3, are presented at different times in Fig. 5. It is seen that by changing the location of the outlet and inlet, the number of suspended particles in the room changes. Therefore, determining the optimal location is very important. In the present study, using the Taguchi method, the optimal location for reducing the number of suspended particles in the room, and the worst location, where the number of suspended is the highest, are determined.

The current study aims to identify the designs that minimize and maximize the number of suspended particles in the room. According to Eqs. (26) and (27), initially, the S/N ratio for the output of each design must be determined. The S/N ratio data for each design is provided in Table 5 for maximizing the number of suspended particles. It should be noted that the value of the S/N ratio for each design to minimize the number of suspended particles is also the same value of the S/N ratio for maximization with a negative sign. The average value of the S/N ratio must be calculated to evaluate the average signal-to-noise ratio value for each parameter at each level.
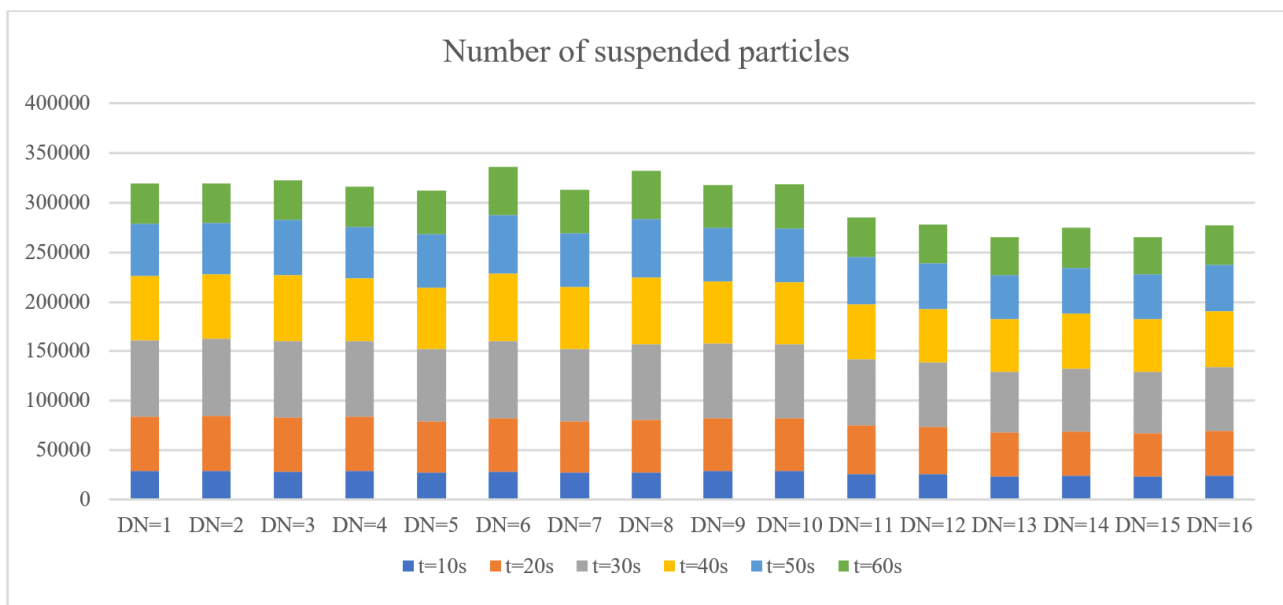

Fig. 5. Number of suspended particles for various designs at different times.

Table 5. The signal-to-noise ratio values for each experiment, considering the maximization of suspended particles in the room (the larger is better).

| # of Exp.	Suspended	SN Ratio	# of Exp.	Suspended	SN Ratio
Test1	40055	$-10*\log\left(\frac{1}{40055^2}\right)=92.053$	Test9	43558	$-10*\log\left(\frac{1}{43558^2}\right)=92.781$
Test2	39322	$-10*\log\left(\frac{1}{39322^2}\right)=91.893$	Test10	44503	$-10*\log\left(\frac{1}{44503^2}\right)=92.968$
Test3	39859	$-10*\log\left(\frac{1}{39859^2}\right)=92.011$	Test11	39833	$-10*\log\left(\frac{1}{39833^2}\right)=92.005$
Test4	40318	$-10*\log\left(\frac{1}{40318^2}\right)=92.110$	Test12	38647	$-10*\log\left(\frac{1}{38647^2}\right)=91.742$
Test5	43636	$-10*\log\left(\frac{1}{43636^2}\right)=92.797$	Test13	37514	$-10*\log\left(\frac{1}{37514^2}\right)=91.484$
Test6	48141	$-10*\log\left(\frac{1}{43636^2}\right)=93.650$	Test14	39733	$-10*\log\left(\frac{1}{39733^2}\right)=91.983$
Test7	44056	$-10*\log\left(\frac{1}{44056^2}\right)=92.880$	Test15	37735	$-10*\log\left(\frac{1}{37735^2}\right)=91.535$
Test8	48339	$-10*\log\left(\frac{1}{48339^2}\right)=93.686$	Test16	39826	$-10*\log\left(\frac{1}{39826^2}\right)=92.003$
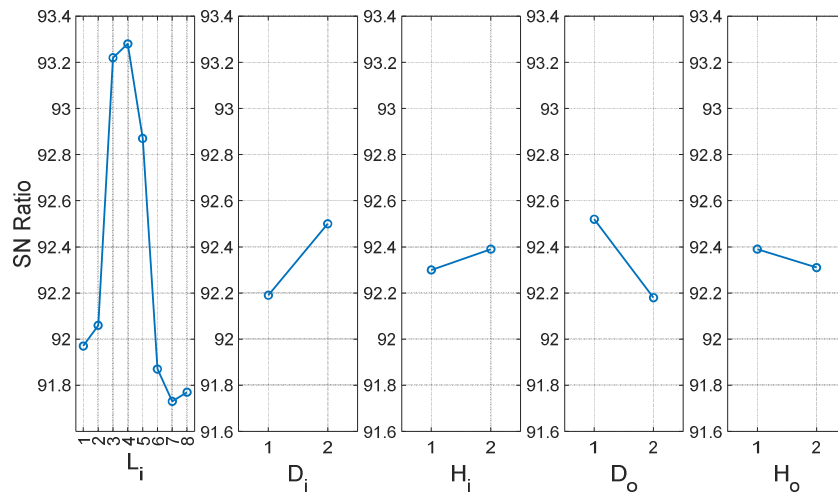
Fig. 6. The S/N Ratio values considering maximizing the number of suspended particles in the room (the larger is better).
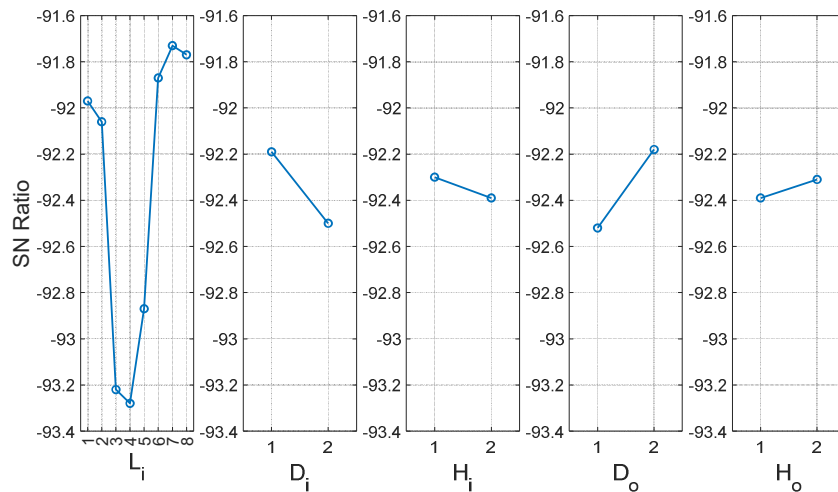

Fig. 7. The S/N Ratio values considering the minimization of the number of suspended particles in the room (the smaller is better).

Figures 6 and 7 depict the S/N ratio values for two cases of maximizing and minimizing the number of suspended particles in the room, respectively (Details presented in Appendix A).

According to the Taguchi method theory, the maximum value of the S/N ratio should be selected at each level to find the optimal value. The optimal levels for each problem parameter, considering the maximization and minimization of the number of suspended particles in the room, are shown in Table 6.

Therefore, based on the data in Table 6, to maximize the number of suspended particles in the room (the worst case), the optimal value for parameter L_i is at level 4, $L_i = 0.257$ m, for parameter D_i is at level 2, $D_i = 0.392$ m, for parameter H_i is at level 2, $H_i = 0$ m, for parameter D_o is at level 1, $D_o = 0.164$ m, and for parameter H_o is at level 1, $H_o = 0.305$ m, which is shown in Fig. 8. Furthermore, to minimize the number of suspended particles in the room (the best case), the optimal value for parameter L_i is at level 7, $L_i = 0.458$ m, for parameter D_i is at level 1, $D_i = 0.164$ m, for parameter H_i is at level 1, $H_i = 0.305$ m, for parameter D_o is at level 2, $D_o = 0.392$ m, and for parameter H_o is at level 2, $H_o = 0$ m, which is shown in Fig. 9.

Table 6. The optimal levels for maximization and minimization of the number of suspended particles in the room.

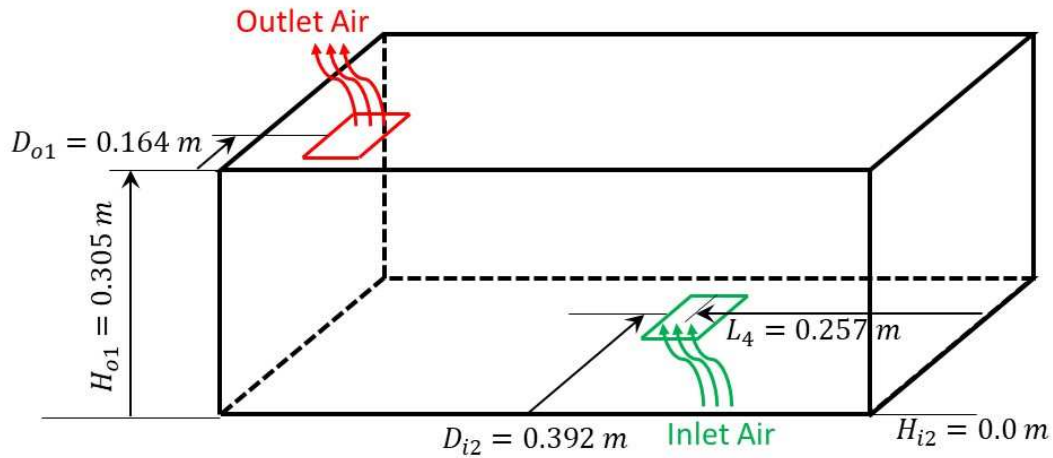| Parameter	L_i	D_i	H_i	D_o	H_o
Maximization (the worst)	4	2	2	1	1
Minimization (the best)	7	1	1	2	2

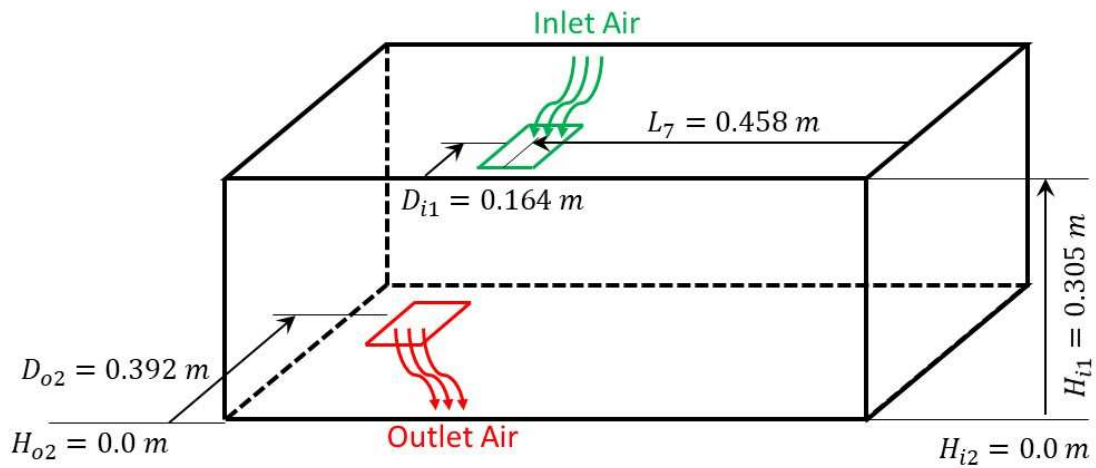**Fig. 8.** Schematic of the inlet and outlet location to maximize the number of suspended particles.

Fig. 9. Schematic of the inlet and outlet location to minimize the number of suspended particles.
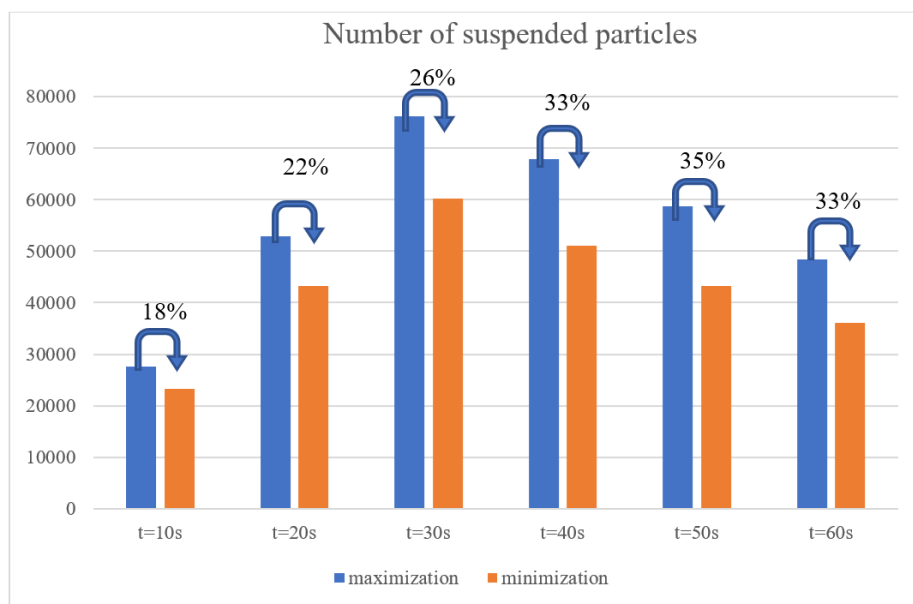
Fig. 10. Number of suspended particles for maximized and minimized cases at different times.

Based on the obtained data and the selection of optimal levels, it is necessary to conduct a new simulation to measure the number of suspended particles in the room. Table 6 shows that the coordinates of the state with the highest number of suspended particles correspond to experiment number 8. Therefore, a new simulation for this state is not necessary, and the results of experiment number 8 are utilized. Figure 10 presents the relevant results for the optimal states at different time intervals. As it is obvious in Fig. 10, the number of suspended particles will change around 30% by changing the position of the ventilation system, so it would be very important to choose a proper situation. Also, the difference of suspended particles will increase by time.

5. Conclusions

In the current study, the optimization of the air inlet and outlet location was carried out using the Taguchi method to reduce the level of suspended particles in the room. The worst-case scenario regarding the maximum number of suspended particles in the room was also investigated. The conclusions of the current study, based on the obtained results, are as follows:

- Using the Taguchi optimization technique, the lattice Boltzmann method for predicting particle motion and optimizing the air inlet and outlet locations showed promising results. It is concluded that this approach could find applications for controlling virus transmission in indoor environments.
- Using the Taguchi optimization method decreases the computational time by more than 87% compared to the full factorial method.
- When the inlet register is on the ceiling and the outlet register is on the floor, indoor air quality is improved.
- The optimal placement of the air inlet and outlet to reduce the number of suspended particles in the room and subsequently reduce the exposure to particles (best case scenario) is as follows (Fig. 9): $L_i = 0.458$ m, $D_i = 0.164$ m, $H_i = 0.305$ m, $D_o = 0.392$ m, $H_o = 0$ m.
- The optimal placement of the air inlet and outlet to increase the number of suspended particles in the room and subsequently increase the exposure to particles (worst case scenario) is as follows (Fig. 8): $L_i = 0.257$ m, $D_i = 0.392$ m, $H_i = 0$ m, $D_o = 0.164$ m, $H_o = 0.305$ m.

Author Contributions

H. Sajjadi planned the scheme, initiated the project, wrote the article draft, and analyzed the results; S.N. Nabavi analyzed the optimization results; G. Ahmadi analyzed the results of particle motion; A. Amiri Delouei developed the LBM method; H. Naeimi developed the DOE method. The manuscript was written through the contribution of all authors. All authors discussed the results reviewed, edited, and approved the final version of the manuscript.

Conflict of Interest

The authors declared no potential conflicts of interest concerning the research, authorship, and publication of this article.

Data Availability Statements

The datasets generated and/or analyzed during the current study are available from the corresponding author upon reasonable request.

Appendix A

The S/N ratio for the output of each test was previously given in Table 5. This appendix gives the average S/N ratio for each parameter at each level. Since level 1 of parameter L_i only exists in experiments 1 and 2, the average S/N ratio for these experiments obtained as follows:

$$SN_{L_{i,1}} = \frac{(92.0531 + 91.8927)}{2} = 91.9729 \tag{A-1}$$

Similarly, the remaining average S/N ratio values for the parameter L_i and the remaining levels can be obtained as follows:

$$SN_{L_{i,2}} = \frac{(92.011 + 92.110)}{2} = 92.061 \tag{A-2}$$

$$SN_{L_{i,3}} = \frac{(92.797 + 93.650)}{2} = 93.224 \tag{A-3}$$

$$SN_{L_{i,4}} = \frac{(92.880 + 93.686)}{2} = 93.283 \tag{A-4}$$

$$SN_{L_{i,5}} = \frac{(92.781 + 92.968)}{2} = 92.875 \tag{A-5}$$

$$SN_{L_{i,6}} = \frac{(92.005 + 91.742)}{2} = 91.874 \tag{A-6}$$

$$SN_{L_{i,7}} = \frac{(91.484 + 91.983)}{2} = 91.734 \tag{A-7}$$

$$SN_{L_{i,8}} = \frac{(91.535 + 92.003)}{2} = 91.769 \tag{A-8}$$

The average S/N ratio values for the parameter D_i and its two levels have been calculated below:

$$SN_{D_{i,1}} = \frac{(92.053 + 92.011 + 92.797 + 92.880 + \ldots + 91.535)}{8} = 92.19 \tag{A-9}$$

$$SN_{D_{i,2}} = \frac{(91.893 + 92.110 + 93.650 + \ldots + 92.003)}{8} = 92.50 \tag{A-10}$$

For the parameter H_i and for its two levels, we have:

$$SN_{H_{i,1}} = \frac{(92.053 + 92.011 + 92.797 + \ldots + 92.003)}{8} = 92.30 \tag{A-11}$$

$$SN_{H_{i,2}} = \frac{(91.893 + 92.110 + 93.650 + \ldots + 91.535)}{8} = 92.39 \tag{A-12}$$

For the parameter D_o:

$$SN_{D_{o,1}} = \frac{(92.053 + 92.011 + 93.650 + \ldots + 92.003)}{8} = 92.52 \tag{A-13}$$

$$SN_{D_{o,2}} = \frac{(91.893 + 92.110 + 92.797 + \ldots + 91.535)}{8} = 92.18 \tag{A-14}$$

And finally, for the parameter H_o:

$$SN_{H_{o,1}} = \frac{(92.053 + 92.011 + 93.650 + \ldots + 91.535)}{8} = 92.39 \tag{A-15}$$

$$SN_{H_{o,2}} = \frac{(91.893 + 92.110 + 92.797 + \ldots + 92.003)}{8} = 92.31 \tag{A-16}$$

References

[1] Sukop, M., Thorne, D., *Lattice Boltzmann modeling: an introduction for geoscientists and engineers*, Springer, 2005.

[2] Succi, S., *The lattice Boltzmann equation: for fluid dynamics and beyond*, Oxford University Press, 2001.

[3] Chen, S., Doolen, G.D., Lattice Boltzmann method for fluid flows, *Annual Review of Fluid Mechanics*, 30(1), 1998, 329-364.

[4] Rahman, A., Redwan, D.A., Thohura, S., Kamrujjaman, M., Molla, M.M., Natural convection and entropy generation of non-Newtonian nanofluids with different angles of external magnetic field using GPU accelerated MRT-LBM, *Case Studies in Thermal Engineering*, 30, 2022, 101769.

[5] Wang, L., Liu, Z., Rajamuni, M., Recent progress of lattice Boltzmann method and its applications in fluid-structure interaction, *Proceedings of the Institution of Mechanical Engineers, Part C: Journal of Mechanical Engineering Science*, 237(11), 2023, 2461-2484.

[6] Liu, W., Wu, C.-Y., Modelling complex particle–fluid flow with a discrete element method coupled with lattice Boltzmann methods (DEM-LBM), *ChemEngineering*, 4(4), 2020, 55.

[7] Mohammadifar, H., Sajjadi, H., Rahnama, M., Jafari, S., Wang, Y., Investigation of nanofluid natural convection heat transfer in open ended L-shaped cavities utilizing LBM, *Journal of Applied and Computational Mechanics*, 7(4), 2021, 2064-2083.

[8] Sajjadi, H., Atashafrooz, M., Delouei, A.A., Wang, Y., The effect of indoor heating system location on particle deposition and convection heat transfer: DMRT-LBM, *Computers & Mathematics with Applications*, 86, 2021, 90-105.

[9] Sajjadi, H., Ahmadi, G., Amiri Delouei, A., Effect of inlet air locations on particle concentration using large eddy simulation based on multi relaxation time lattice Boltzmann method, *Journal of Applied and Computational Mechanics*, 7(4), 2021, 1944-1955.

[10] Sugaya, K., Imamura, T., Turbulent flow simulations of the common research model on Cartesian grids using recursive fitting approach, *Journal of Computational Physics*, 467, 2022, 111460.

[11] Brenner, O., Piroozmand, P., Jenny, P., Efficient assimilation of sparse data into RANS-based turbulent flow simulations using a discrete adjoint method, *Journal of Computational Physics*, 471, 2022, 111667.

[12] Vandenhoeck, R., Lani, A., Steelant, J., Development of an implicit high-order flux reconstruction solver for the Langtry-Menter Laminar-Turbulent Transition RANS model, *Computer Physics Communications*, 278, 2022, 108408.

[13] Rosas, R.H., Wang, B.-C., DNS Study of turbulent heat transfer in an elliptical pipe flow subjected to system rotation about the major axis, *International Journal of Heat and Mass Transfer*, 184, 2022, 122230.

[14] Sajjadi, H., Salmanzadeh, M., Ahmadi, G., Jafari, S., LES and RANS model based on LBM for simulation of indoor airflow and particle dispersion and deposition, *Building and Environment*, 102, 2016, 1-12.

[15] Balachandar, S., Zaleski, S., Soldati, A., Ahmadi, G., Bourouiba, L., Host-to-host airborne transmission as a multiphase flow problem for science-based social distance guidelines, *International Journal of Multiphase Flow*, 132, 2020, 103439.

[16] Gorbunov, B., Aerosol particles generated by coughing and sneezing of a SARS-CoV-2 (COVID-19) host travel over 30 m distance, *Aerosol and Air Quality Research*, 21(3), 2021, 200468.

[17] Bahramian, A., Mohammadi, M., Ahmadi, G., Effect of indoor temperature on the velocity fields and airborne transmission of sneeze droplets: An experimental study and transient CFD modeling, *Science of The Total Environment*, 858, 2023, 159444.

[18] Bahramian, A., Ahmadi, G., Effect of sneeze flow velocity profiles on the respiratory droplets dispersion in a confined space: An experimental and

computational fluid dynamics study, *Physics of Fluids*, 35(6), 2023, 063330.

[19] Karami, S., Lakzian, E., Ahmadi, G., Prediction of COVID-19 infection in dental clinic by CFD and wells-riley model, identifying safe area and proper ventilation velocity, *International Journal of Refrigeration*, 151, 2023, 112-124.

[20] Harish, S., Nihaarikha, G., Harish, R., Computational study of Corona virus diffusion in a closed environment, *in: IOP Conference Series: Materials Science and Engineering*, IOP Publishing, 2021.

[21] Mirzaie, M., Lakzian, E., Khan, A., Warkiani, M.E., Mahian, O., Ahmadi, G., COVID-19 spread in a classroom equipped with partition–A CFD approach, *Journal of Hazardous Materials*, 420, 2021, 126587.

[22] Mofakham, A.A., Ahmadi, G., On random walk models for simulation of particle-laden turbulent flows, *International Journal of Multiphase Flow*, 122, 2020, 103157.

[23] Ahmed, T., Wendling, H.E., Mofakham, A.A., Ahmadi, G., Helenbrook, B.T., Ferro, A.R., Brown, D.M., Erath, B.D., Variability in expiratory trajectory angles during consonant production by one human subject and from a physical mouth model: Application to respiratory droplet emission, *Indoor Air*, 31(6), 2021, 1896-1912.

[24] Mofakham, A.A., Helenbrook, B.T., Erath, B.D., Ferro, A.R., Ahmed, T., Brown, D.M., Ahmadi, G., On the variation of fricative airflow dynamics with vocal tract geometry and speech loudness, *Aerosol Science and Technology*, 56(5), 2022, 446-460.

[25] Mofakham, A.A., Helenbrook, B.T., Erath, B.D., Ferro, A.R., Ahmed, T., Brown, D.M., Ahmadi, G., Influence of two-dimensional expiratory airflow variations on respiratory particle propagation during pronunciation of the fricative [f], *Journal of Aerosol Science*, 173, 2023, 106179.

[26] Obeid, S., White, P., Rosati Rowe, J., Ilacqua, V., Rawat, M.S., Ferro, A.R., Ahmadi, G., Airborne respiratory aerosol transport and deposition in a two-person office using a novel diffusion-based numerical model, *Journal of Exposure Science & Environmental Epidemiology*, 2023, https://doi.org/10.1038/s41370-023-00546-w.

[27] Karami, S., Lakzian, E., Shabani, S., Dykas, S., Salmani, F., Lee, B.J., Warkiani, M.E., Kim, H.D., Ahmadi, G., Selecting the safe area and finding proper ventilation in the spread of the COVID-19 virus, *Energies*, 16(4), 2023, 1672.

[28] Muthusamy, J., Haq, S., Akhtar, S., Alzoubi, M.A., Shamim, T., Alvarado, J., Implication of coughing dynamics on safe social distancing in an indoor environment—A numerical perspective, *Building and Environment*, 206, 2021, 108280.

[29] Ahmadzadeh, M., Shams, M., A numerical approach for preventing the dispersion of infectious disease in a meeting room, *Scientific Reports*, 12(1), 2022, 16959.

[30] Xu, A., Tao, S., Shi, L., Xi, H.D., Transport and deposition of dilute microparticles in turbulent thermal convection, *Physics of Fluids,* 32, 2020, 083301.

[31] Kechagias, J., Kitsakis, K., Vaxevanidis, N., Comparison of full versus fractional factorial experimental design for the prediction of cutting forces in turning of a titanium alloy: A case study, *International Journal of Materials*, 4, 2017, 1-4.

[32] Fountas, N., Aslani, K.-E., Kechagias, J., Kyratsis, P., Vaxevanidis, N., Experimental and statistical study of surface roughness in CNC slot milling of AL 7075 alloy using full and fractional factorial design, *Tribology in Industry*, 43(4), 2022, 283-293.

[33] Karna, S.K., Sahai, R., An overview on Taguchi method, *International Journal of Engineering and Mathematical Sciences*, 1(1), 2012, 1-7.

[34] Freddi, A., Salmon, M., *Design principles and methodologies: From conceptualization to first prototyping with examples and case studies*, Springer, 2018.

[35] d'Humières, D., Multiple–relaxation–time lattice Boltzmann models in three dimensions, *Philosophical Transactions of the Royal Society of London. Series A: Mathematical, Physical and Engineering Sciences*, 360(1792), 2002, 437-451.

[36] Li, A., Ahmadi, G., Dispersion and deposition of spherical particles from point sources in a turbulent channel flow, *Aerosol Science and Technology*, 16(4), 1992, 209-226.

[37] Posner, J., Buchanan, C., Dunn-Rankin, D., Measurement and prediction of indoor air flow in a model room, *Energy and Buildings*, 35(5), 2003, 515-526.

[38] Tian, Z.F., Tu, J.Y., Yeoh, G., Yuen, R., On the numerical study of contaminant particle concentration in indoor airflow, *Building and Environment*, 41(11), 2006, 1504-1514.

ORCID iD

H. Sajjadi https://orcid.org/0000-0002-0681-7682

S.N. Nabavi https://orcid.org/0000-0002-1531-8957

G. Ahmadi https://orcid.org/0000-0001-5277-7960

A. Amiri Delouei https://orcid.org/0000-0001-7414-4195

H. Naeimi https://orcid.org/0000-0003-2710-7943

How to cite this article: Sajjadi H. et al., Optimization of Ventilation Register Locations for Reducing Suspended Particle Concentration Using the Taguchi Method, *J. Appl. Comput. Mech.*, xx(x), 2024, 1–12. https://doi.org/10.22055/jacm.2024.46267.4488

Publisher's Note Shahid Chamran University of Ahvaz remains neutral with regard to jurisdictional claims in published maps and institutional affiliations.